



GENETICS

DNA cytosine methylation suppresses meiotic recombination at the sex-determining region

Tong Ge^{1†}, Xiuqi Gui^{2†}, Jia-Xi Xu^{1†}, Wei Xia^{1†}, Chao-Han Wang¹, Wenqiang Yang^{3,4}, Kaiyao Huang⁵, Colum Walsh⁶, James G. Umen⁷, Jörn Walter⁸, Ya-Rui Du¹, Hui Chen^{1*}, Zhen Shao^{2*}, Guo-Liang Xu^{1,9*}

Meiotic recombination between homologous chromosomes is vital for maximizing genetic variation among offspring. However, sex-determining regions are often rearranged and blocked from recombination. It remains unclear whether rearrangements or other mechanisms might be responsible for recombination suppression. Here, we uncover that the deficiency of the DNA cytosine methyltransferase DNMT1 in the green alga *Chlamydomonas reinhardtii* causes anomalous meiotic recombination at the mating-type locus (*MT*), generating haploid progeny containing both *plus* and *minus* mating-type markers due to crossovers within *MT*. The deficiency of a histone methyltransferase for H3K9 methylation does not lead to anomalous recombination. These findings suggest that DNA methylation, rather than rearrangements or histone methylation, suppresses meiotic recombination, revealing an unappreciated biological function for DNA methylation in eukaryotes.

INTRODUCTION

Sexual reproduction fuels genetic diversity for natural selection and can remove deleterious mutations from a population. Separate mating types or sexes can increase the efficiency of recombination by ensuring that matings only take place between nonidentical individuals in a population. Sexual dimorphism is also prevalent across eukaryotes and is often controlled genetically through a sex-determining region (SDR). Once formed, SDRs may accumulate genes or alleles that have sex-specific or mating-type-specific roles, and once this occurs, there is selection to maintain linkage of these genes with the SDR. Thus, a hallmark feature of SDRs is suppressed recombination that is typically accompanied by structural rearrangements between the two SDR haplotypes. Diverse mechanisms, including inversions in DNA sequences, recombination modifiers, and epigenetic changes, have been proposed to suppress recombination in the SDR (1). There is compelling evidence that histone modifications, such as histone deacetylation and H3K9 methylation, act to prevent recombination in the SDR in yeasts (2). However, early eukaryotes lack chromatin and histone modifications (3); therefore, the role of epigenetic mechanisms in suppression of recombination in the SDR of these organisms is unclear.

Chlamydomonas reinhardtii (*Chlamydomonas*) is a free-living, haploid unicellular green alga and an important reference organism for sexual cycle research (4). Moreover, *C. reinhardtii* has two mating types, *plus* (*mt+*) and *minus* (*mt-*), which are defined by distinct haplotypes at the mating-type (*MT*) locus (4). The *MT* locus is a genetically complex chromosomal region encompassing ~211 kb (*mt-*) or 375 kb (*mt+*) of DNA, which is rearranged between the two mating-type haplotypes. The sequence rearrangements presumably contribute to recombination suppression at *MT* though additional mechanisms to suppress recombination may also exist (5). However, it has remained a challenge to determine whether these rearrangements reflect the consequence of low recombination activity or are the cause of recombination suppression. Furthermore, epigenetic factors that potentially confer recombinational suppression at *MT* in *C. reinhardtii* have not been examined.

DNA cytosine methylation is a common base modification found in most eukaryotic groups and plays an essential role in diverse types of genome regulation, including silencing of retroelements, genomic imprinting, X chromosome inactivation, and heterochromatin stability (6, 7). *C. reinhardtii* has a relatively low amount of 5mC in its nuclear genome (~0.4% of total cytosine) compared with plants and animals, and the function of nuclear 5mC in this alga is unknown. *C. reinhardtii* encodes six putative cytosine methyltransferase genes in its genome that may contribute to nuclear and/or chloroplast DNA methylation (8).

Here, we sought to identify the DNA cytosine methyltransferase responsible for nuclear DNA methylation in *C. reinhardtii* and found that DNA methyltransferase 1 (DNMT1) (Cre10.g461750) was the major maintenance methyltransferase. A null mutation in *dnmt1* removed 95% of nuclear 5mC and had an unexpected phenotype of illegitimate meiotic recombination between the *mt+* and *mt-* haplotypes. These findings establish an essential role for 5mC in recombination suppression at *MT*, thus expanding the biological significance of DNA methylation. These data also show that rearrangements between SDR haplotypes are insufficient to block recombination and may initially be a consequence rather than cause of recombination suppression. Notably, a typically heterochromatic histone modification, histone H3 lysine-9 methylation (H3K9me1),

¹Key Laboratory of Epigenetic Regulation and Intervention, Chinese Academy of Sciences Center for Excellence in Molecular Cell Science, Shanghai Institute of Biochemistry and Cell Biology, Chinese Academy of Sciences, University of Chinese Academy of Sciences, Shanghai 200031, China. ²CAS Key Laboratory of Computational Biology, Shanghai Institute of Nutrition and Health, Chinese Academy of Sciences, Shanghai 200031, China. ³Photosynthesis Research Center, Key Laboratory of Photobiology, Institute of Botany, Chinese Academy of Sciences, Beijing 100093, China. ⁴China National Botanical Garden, Beijing 100093, China. ⁵Key Laboratory of Algal Biology, Institute of Hydrobiology, Chinese Academy of Sciences, Wuhan 430072, China. ⁶Department of Cell Biology, Institute for Biomedical and Clinical Sciences, Linköping University, Linköping, Sweden. ⁷Donald Danforth Plant Science Center, 975 N. Warson Rd, St. Louis, MO 63132, USA. ⁸Department of Genetics/Epigenetics, Saarland University, Saarbrücken 66123, Germany. ⁹Key Laboratory of Medical Epigenetics and Metabolism, Institutes of Biomedical Sciences, Shanghai Medical College, Chinese Academy of Medical Sciences (RU069) and Zhongshan-Xuhui Hospital, Fudan University, Shanghai 200032, China.

*Corresponding author. Email: chenhui01@sibs.ac.cn (H.C.); shaozhen@sinh.ac.cn (Z.S.); glxu@sibcb.ac.cn (G.-L.X.)

†These authors contributed equally to this work.

Copyright © 2024 the Authors, some rights reserved; exclusive licensee American Association for the Advancement of Science. No claim to original U.S. Government Works. Distributed under a Creative Commons Attribution NonCommercial License 4.0 (CC BY-NC).

Downloaded from https://www.science.org at Shanghai Information Center for Life Sciences, CAS on October 09, 2024

is reduced in *dnmt1* mutants, but mutation of the gene responsible for H3K9 methylation in a DNMT1 wild-type (WT) background did not alleviate recombination suppression at *MT*.

RESULTS

DNMT1 functions as a maintenance DNA cytosine methyltransferase in *C. reinhardtii*

Among six DNMT paralogs encoded in the genome of *C. reinhardtii*, we focused on three that are predicted to encode nuclear DNA cytosine methyltransferases (8): Cre10.g461750, Cre03.g202150, and Cre03.g200750. These three DNMTs were categorized into two branches in a DNMT phylogeny (fig. S1A). Cre10.g461750 grouped with the maintenance methyltransferases MET1 in *Arabidopsis thaliana* and Dnmt1 in mouse, and besides, its methyltransferase domain contains predicted replication focus targeting sequence (RFTS) and bromo-adjacent homology (BAH) domains (Fig. 1A), suggesting that it might be a maintenance enzyme in *C. reinhardtii*. We therefore designated Cre10.g461750 as CrDNMT1. The other two putative nuclear methyltransferases, Cre03.g202150 and Cre03.g200750, grouped with the DNMT2 family. Both contain unique long N- and C-terminal sequences in addition to the conserved methyltransferase domain in the middle, different from the canonical DNMT2 containing a methyltransferase domain only (fig. S1B).

To determine whether these three potential nuclear DNA cytosine methyltransferases are responsible for DNA methylation in

C. reinhardtii, we obtained pre-existing insertion alleles from the *Chlamydomonas* Library Project (CLiP) (9) or made CRISPR-mediated gene edits (Fig. 1, B and C, and fig. S1C). Using ultrahigh-performance liquid chromatography–tandem mass spectrometry (UHPLC-MS/MS) analysis, we quantified 5mC at 0.37% of total C in the total DNA of WT strain (Fig. 1C). In *dnmt1* Ins1 strain (from CLiP), the 5mC level was reduced by more than 95% (Fig. 1C), while it was unchanged in the mutant strains deficient in the other two potential DNMTs (fig. S1C). To verify that the reduction of 5mC is due to *DNMT1* deficiency, we used CRISPR-Cas9 gene editing to generate an insertional mutation in exon 2 (*dnmt1* Ins2; Fig. 1B) and a single-amino acid point mutation (C1830S) to disrupt the PCQ catalytic motif conserved in all cytosine methyltransferases. Both mutants showed diminished 5mC levels similar to the *dnmt1* Ins1 strain (Fig. 1C). These results indicate that DNMT1 is the major cytosine methyltransferase of *C. reinhardtii*, and thereafter, we focused on the function of DNMT1.

To investigate whether DNMT1 functions as a maintenance or de novo methyltransferase through the life cycle of *C. reinhardtii*, we crossed a *dnmt1* mutant strain with a *DNMT1* WT strain and assessed the methylation level in four meiotic progenies from a tetrad. As expected, the two *dnmt1* progenies had low levels of methylation (~0.05%) similar to the *dnmt1* parental strain (Fig. 1D). The 5mC level in the two *DNMT1* WT progenies was about half of that in the *DNMT1* parental strain (Fig. 1D). This finding is consistent with random segregation of methylated and unmethylated DNA from

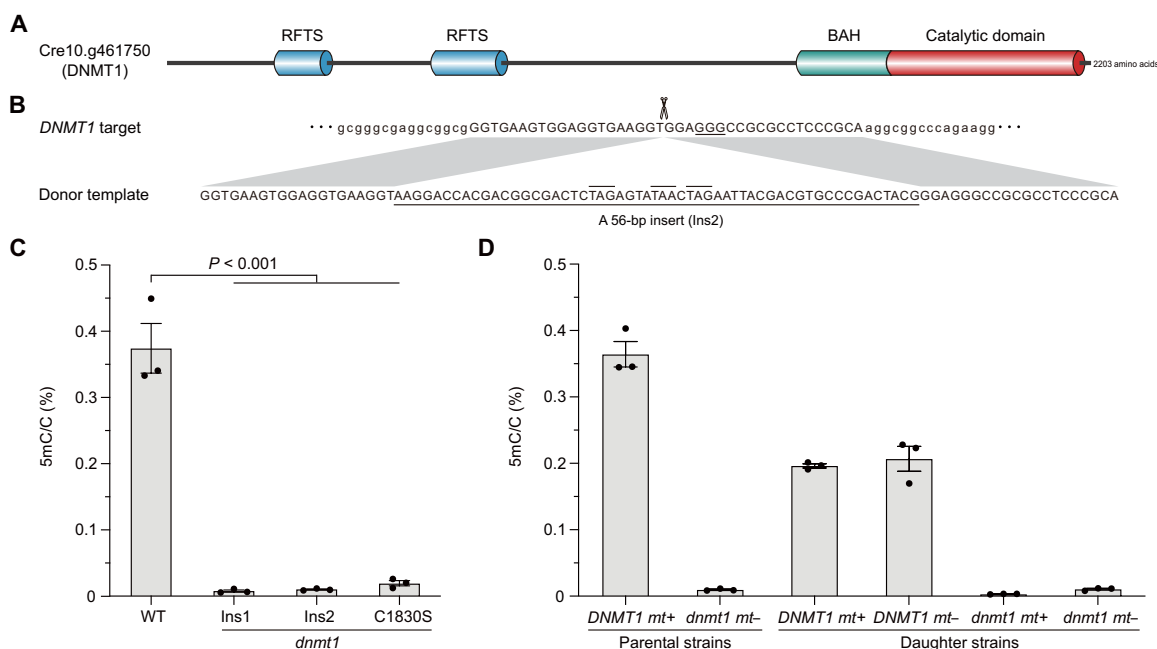


Fig. 1. Functional characterization of a maintenance DNMT. (A) Domain architecture of the DNMT1 protein. The predicted RFTS domains, BAH domain, and C-terminal catalytic domain are indicated. (B) Generation of *dnmt1* mutations based on targeted gene inactivation using CRISPR-Cas9 technology in WT CC-5325 strain. A 56-bp insert (Ins2) containing three stop codons (overlined) is introduced into exon 2 of the *DNMT1* gene by microhomologous recombination using the indicated donor template. The protospacer adjacent motif (PAM) is underlined, and the Cas9 cleavage site is indicated with scissors. (C) 5mC nucleoside contents in the total DNA from CC-5325 WT strain and three independent *dnmt1* mutant strains quantified by mass spectrometry (MS). The *dnmt1* Ins1 strain obtained from CLiP carries a 2219-bp frameshifting insertion within exon 9. The *dnmt1* Ins2 strain was gene edited (B). The *dnmt1* C1830S strain contains a cysteine-to-serine point mutation in the PCQ motif of the catalytic domain. (D) 5mC nucleoside contents in total DNA quantified by MS from WT CC-5155 (*mt+*), *dnmt1* Ins2 (*mt-*) parental strains, and their four daughter strains obtained from one heterozygote. [(C) and (D)] Data are means \pm SEM from three independent technical replicates (dots). Two-tailed Student's *t* test was used without adjustment for multiple comparisons (C).

the two parents and the ability of DNMT1 to maintain methylated DNA inherited from the WT parent but inability to remethylate sequences inherited from the *dnmt1* parent. Together, these data indicate that DNMT1 acts as a maintenance methyltransferase and lacks de novo methyltransferase activity on unmethylated DNA.

Reduction in spore viability and formation of spores with mixed mating type

Despite their substantial loss of 5mC, the *dnmt1* strains did not display noticeable growth defects under autotrophic or heterotrophic conditions (fig. S2A). To determine whether the sexual cycle is normal in *dnmt1* strains, we performed pairwise crosses with WT and *dnmt1* strains of each mating type. In crosses where either parent was WT, spore viability was over 80% (Fig. 2A). However, in

dnmt1 × *dnmt1* crosses, spore viability was reduced to 68% (Fig. 2A). The *dnmt1* homozygotes tended to produce fewer four-spore-viable tetrads (73 to 53%) but more three-spore- (20 to 30%) and two-spore-viable (8 to 18%) tetrads than the WT homozygotes after meiosis (Fig. 2B).

The decreased spore viability in *dnmt1* × *dnmt1* progeny might be caused by increases in meiotic nondisjunction and/or illegitimate recombination events. In genotyping of mating-type markers in progeny from three-spore-viable or two-spore-viable tetrads in *dnmt1* × *dnmt1* crosses, we found an abnormally high frequency of progeny that carried both *mt+* and *mt-* markers, *FUS1* and *MID1*, respectively (Fig. 2C). To rule out the possibility of mixed colonies, we repeated this analysis using subcloned single cells (fig. S2B) and confirmed five *mt+/-* colonies among the progeny of 212 *dnmt1*

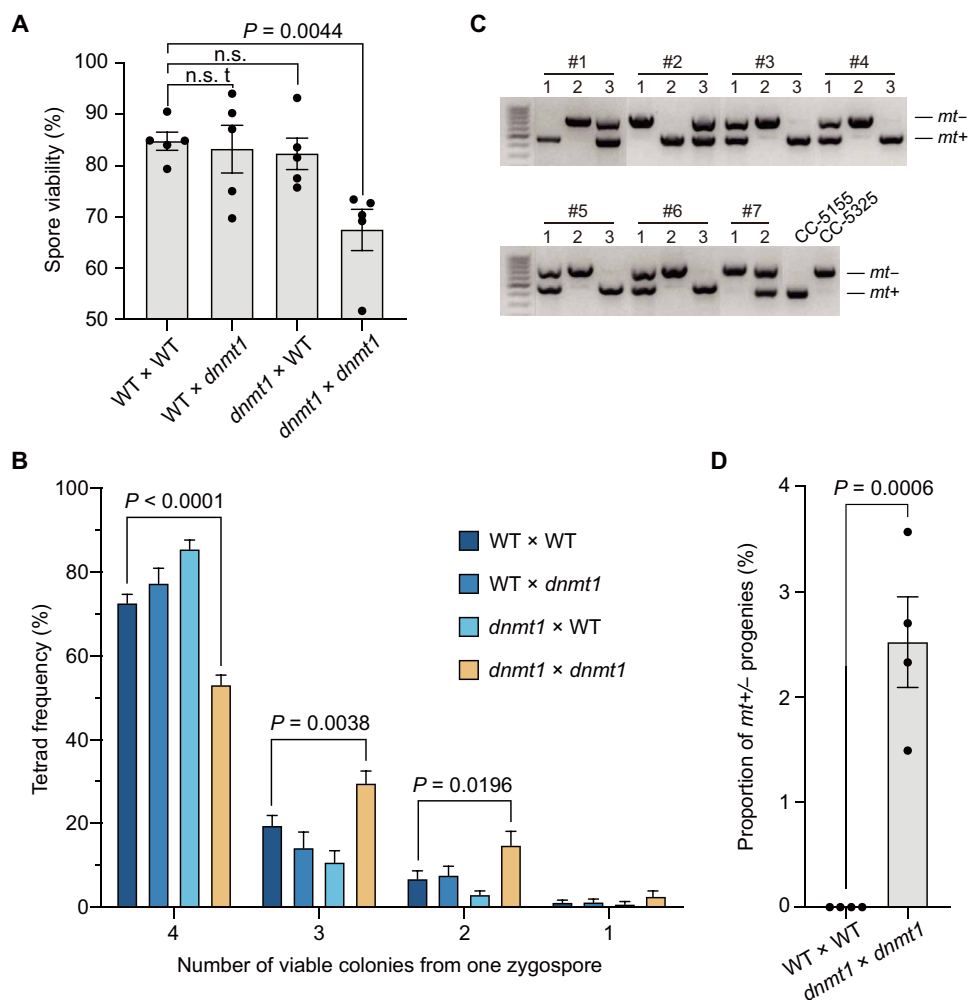


Fig. 2. Meiotic defects of *dnmt1* homozygotes. (A) Spore viability of WT homozygotes, two types of heterozygotes [WT (*mt+*) × *dnmt1* (*mt-*) and *dnmt1* (*mt+*) × WT (*mt-*)], and *dnmt1* homozygotes. Spore viability was calculated by dividing the number of obtained progeny colonies by the number of spores placed on the plate. WT (*mt+*) and WT (*mt-*) were CC-5155 strain and CC-5325 strain, respectively. *dnmt1* (*mt+*) was from *dnmt1* Ins1 strain (*mt-*) (Fig. 1C) backcrossed with WT CC-5155 strain (*mt+*); *dnmt1* (*mt-*) strain was from *dnmt1* Ins2 strain (*mt-*) (Fig. 1C) backcrossed with WT CC-5155 strain (*mt+*). n.s., not significant. (B) Frequency of tetrads with one to four viable spore(s) in the four sets of crosses indicated. (C) *MT* genotyping for tetrads containing *mt+/-* strains through *mt*-specific genes (*FUS1* for *mt+* and *MID1* for *mt-*). The primers were reported previously (43). (D) Proportion of *mt+/-* progenies obtained from WT homozygotes (0 of 177) and *dnmt1* homozygotes (5 of 212). The proportion of *mt+/-* progenies is defined as the ratio of zygospores capable of producing at least one *mt+/-* progeny to the total number of zygospores analyzed. The tested strains are from tetrads with one to three viable spore(s). [(A), (B), and (D)] Data are means ± SEM from five [(A) and (B)] or four (D) independent biological replicates (dots). Two-tailed Student's *t* test was used without adjustment for multiple comparisons.

homozygotes, whereas no *mt+/-* colony emerged from the progeny of 177 WT homozygotes (Fig. 2D).

Meiotic recombination at *MT* occurs in *dnmt1* homozygotes

We tested two possible causes for the anomalous coexistence of markers from two mating types in one offspring cell: illegitimate recombination within the rearranged domain of *MT* resulting in an *MT* chimera with parts from both *mt+* and *mt-*, or nondisjunction of chromosome 6 that carries the *MT* locus, leading to an aneuploid cell with an *mt+* and *mt-* copy of chromosome 6. We performed whole-genome sequencing on the #1-3 strain with mixed mating type. Analysis of chromosome 6 in #1-3 showed a pattern of parental single-nucleotide polymorphisms (SNPs) consistent with a recombination event within *MT* and inconsistent with two copies of chromosome 6 being present. There were

exclusively *mt-* SNPs from chromosome 6 on the telomere proximal side of *MT* and exclusively *mt+* SNPs on the centromere proximal-side *MT* (Fig. 3A). Within the *MT* R-region, only *mt-* SNPs were on the telomere proximal side until gene 522872 (*Cre06.g252600*), after which there were exclusively *mt+* SNPs and sequences in the order found within the *mt+* haplotype. Because the same orientation of gene 522872 in both mating-type haplotypes, this region of the R-region can support a reciprocal exchange, while its location relative to other R-region genes is different in each *MT* haplotype. Recombination in or around this gene would lead to one chromatid losing a group of *MT* genes and the other chromatid gaining a duplication of the same genes. The meiotic recombinant with the deletion would likely be inviable, while the reciprocal recombinant would have a duplicated group of shared genes from both mating types.

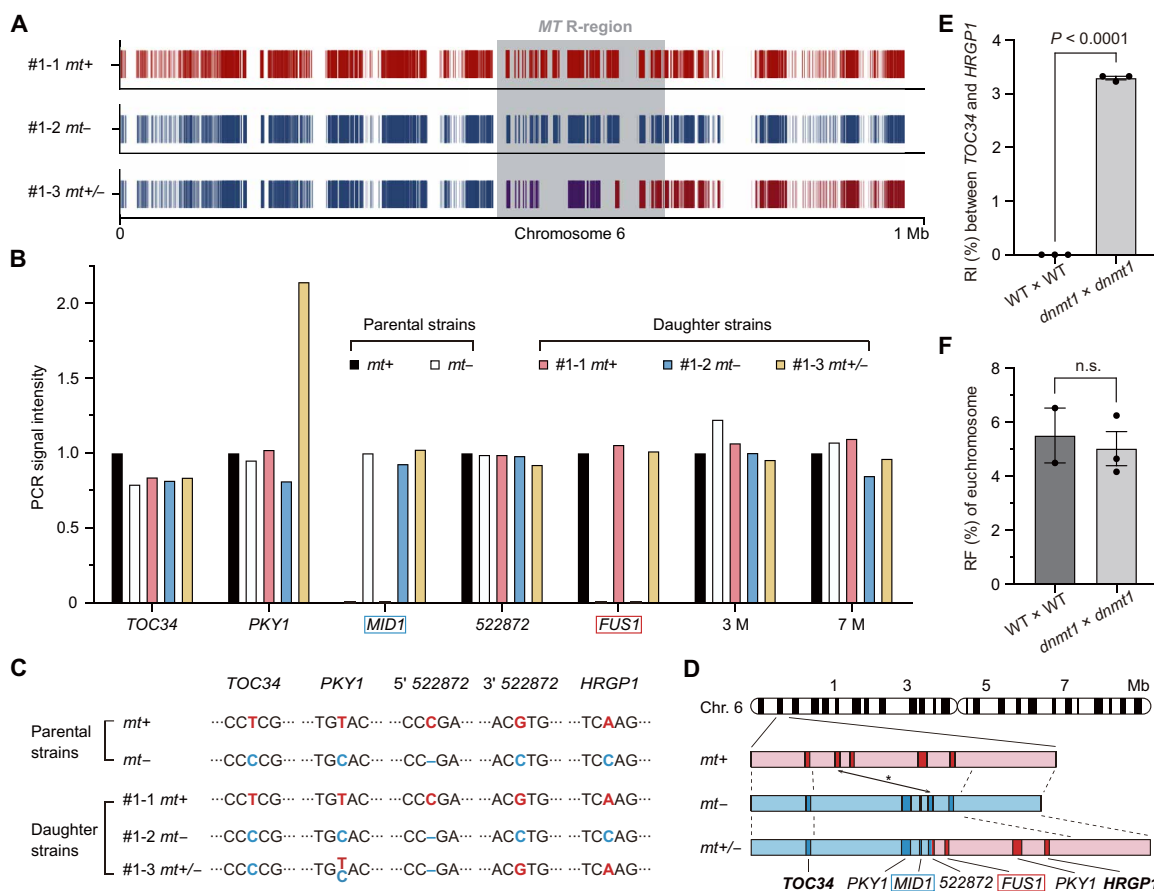


Fig. 3. Aberrant recombination at *MT* in *dnmt1* homozygotes. (A) SNP analysis of chromosome 6 revealing the occurrence of recombination at *MT* in daughter strain #1-3. The shaded area denotes *MT* R-region. Red and blue vertical lines represent SNPs distinguishing between parental *mt+* and *mt-* strains. Purple lines in #1-3 signify the coexistence of both *plus-* and *minus-* specific SNPs within the duplicated sequences in *MT* R-region. (B) Quantitative PCR analysis of genomic DNA from strains of a representative cross to examine the copy number. 3 M and 7 M are at the 3 Mb and 7 Mb loci on chromosome 6, respectively. The y axis shows PCR signal intensity relative to *AGG1*. (C) Mapping of the recombination site. Colored bold letters (red in *mt+* and blue in *mt-*) indicate SNPs present in the DNA sequence of four indicated genes within *MT*. (D) Diagram depicting a meiotic recombination event at *MT* in a *dnmt1* homozygote. Genes located on the *plus* (pink) and *minus* (light blue) *MT* loci are denoted by red and dark blue boxes, respectively. The recombination site within 522872 gene is indicated by a double arrow line with asterisk between chromosomes 6 of *mt+* and *mt-*. (E) Recombination incidence (RI) between *TOC34* and *HRGP1* markers (~250 kb apart) at *MT* in *dnmt1* (91) and WT (91) homozygotes. The incidence was determined by homozygotes which generated one to three viable spore(s). (F) Recombination frequency (RF) of a 257-kb region (chromosome 6, 8,099,433 to 8,357,675) on the right arm of chromosome 6 in *dnmt1* (123) and WT (135) homozygotes. The frequency was determined by homozygotes that generated one to four viable spores. [(E) and (F)] Data are means \pm SEM from two or three independent biological replicates (dots). Two-tailed Student's *t* test was used without adjustment for multiple comparisons.

To further confirm the inferred structure of the recombinant *MT* locus in #1-3 strain, we performed real-time polymerase chain reaction (PCR) on selected *MT* genes from both mating types (Fig. 3B). Notably, the PCR signal intensities of *FUS1* and *MID1* in #1-3 strain were the same as those of chromosome 6 arm regions at the 3 M and 7 M loci, while the signal intensity was doubled for *PKY1*, a gene that is within the duplicated region of *MT*. SNP tracking revealed that the mixed mating-type strain (#1-3) received *TOC34*, one copy of *PKY1*, and 5' region of the gene 522872 from the *mt*⁻ parental strain; whereas *HRGP1*, a second copy of *PKY1*, and 3' region of the gene 522872 were from the *mt*⁺ parental strain (Fig. 3C). On the basis of these observations, we concluded that the 5' region of the gene 522872 from *mt*⁻ had recombined with the 3' region from *mt*⁺ within a 190-bp spacer between the two SNPs, generating an *mt*^{+/-} hybrid *MT* locus (Fig. 3D). Analysis of six additional independently isolated mixed-*mt* strains indicated that all recombinations had occurred within the 522872 gene, although across three different SNP intervals (fig. S3), reflecting a notable constraint for site selection. Our analyses indicate that illegitimate recombination can occur within a restricted portion of the *MT* R-region, and such recombination is also likely to lead to production of some inviable spores due to loss of essential genes within *MT*. As expected, #1-3 strain mated as a *minus* (fig. S4), since *MID1* is a dominant determinant of mating type (4).

Using SNPs in *MT* R-region markers *TOC34* and *HRGP1* we compared recombination rates within *MT* between WT and *dnmt1* homozygotes (Fig. 3E). The recombination incidence in WT was 0%, while in *dnmt1* homozygotes it was 3.3%. The homozygotes carrying the *dnmt1* C1830S point mutation also displayed meiotic defects, characterized by decreased spore viability and a comparable recombination incidence at *MT* (fig. S5). By contrast, DNMT1 deficiency had little effect on meiotic recombination within euchromatic regions as evidenced by the unaltered recombination frequency within a euchromatic fragment of chromosome 6 (Fig. 3F). Therefore, DNA methylation appears to be essential for recombination suppression at *MT* but does not regulate recombination in euchromatin.

Loss of 5mC at *MT* in the *dnmt1* mutant strains

To assess the effect of DNMT1 deficiency on 5mC global distribution, with an emphasis on the *MT*, we performed whole-genome bisulfite sequencing (WGBS) on WT and *dnmt1* strains of both mating types in the vegetative stage. Consistent with previous work (10), most of the 5mCs were found in the CG motif, and at least one heavily methylated region (MR; defined as ≥ 20 -kb regions with $\geq 40\%$ of 5mCG/CG) per chromosome could be identified in the WT strains. However, all of these large hypermethylated regions were lost in the *dnmt1* strains (Fig. 4A, fig. S6A, and table S1). In addition, 555 highly MRs were identified in WT strains, with a median 5mCG/CG ratio of 0.24, ranging in length from 21 to 157,782 bp and averaging 833 CpG sites (see Materials and Methods). Similarly, all MRs became demethylated in the *dnmt1* strains (fig. S6B and table S2).

Notably, the WT strains had a notable amount of methylation at *MT* on chromosome 6, and this was also lost in the *dnmt1* strains (Fig. 4A). This was exemplified by *LPS1* (lipase domain protein, *Cre06.g252800*), the longest gene (~36 kb) in *MT*, which displayed the most pronounced methylation in WT, but it was missing in *dnmt1* strains like methylation elsewhere across the genome (Fig. 4B and fig. S6C). Somewhat unexpectedly, the repeats at *MT* contained

little methylation in WT with the exception of DNA/*Novosib* and short interspersed nuclear element/*tRNA*, which displayed notable levels of 5mC in WT but were devoid of methylation in the mutant strains (fig. S6D).

By taking advantage of SNPs, we tracked the parent of origin of an allele of interest and found that the *LPS1* gene on an *MT* allele originally methylated in the WT parent could remain methylated only when segregated into the DNMT1-proficient daughter strain (Fig. 4C). On the other hand, the region on the unmethylated allele from the DNMT1-deficient parent remained unmethylated even if it was segregated in the DNMT1-proficient daughter strain (Fig. 4C). These observations confirm that DNMT1 is essential for maintaining the inheritance of parental methylation patterns but does not have the de novo methylation activity required to establish new methylation patterns on unmethylated templates. A deficiency in DNMT1 results in widespread loss of methylation across the genome, including the *MT* locus.

Repressive histone methylation H3K9me1 is depleted at *MT* in *dnmt1* strains

Eukaryotic genomes are commonly organized into two forms of chromatin: euchromatin and heterochromatin, though it is not clear whether this binary model applies to *C. reinhardtii* (11). DNA methylation promotes formation of the latter (12). Apart from 5mC, histone modifications are also important determinants of structurally and functionally distinct chromatin states. In *C. reinhardtii*, H3 histones in the transcribed regions of repressed genes contain high levels of monomethylation of lysine-4 (H3K4me1, ~80% of total H3) or lysine-9 (H3K9me1, ~16% of total H3) as repressive marks and low levels of trimethylation of lysine-4 (H3K4me3) or lysine-9 (H3K9me3) as active marks (13–15). To explore whether the meiotic defects caused by *DNMT1* deficiency are accompanied by changes in histone modifications, we used chromatin immunoprecipitation sequencing (ChIP-seq) to profile the genome-wide distribution of five distinct posttranslational modifications of H3 including H3K4me1, H3K9me1, H3K4me3, H3K9me3, and H3K27ac in WT (*mt*⁺), WT (*mt*⁻), *dnmt1* (*mt*⁺), and *dnmt1* (*mt*⁻) strains. Consistent with previous studies (16), H3K4me1, H3K9me1, and H3K27ac signals were enriched in gene bodies, while H3K4me3 and H3K9me3 signals were enriched at promoters near transcription start sites (Fig. 5A). Compared with WT, *dnmt1* had no visible difference in H3K4me1 but a substantial decrease in H3K9me1 and an increase in active modifications (H3K4me3, H3K9me3, and H3K27ac) in MRs (Fig. 5, A and B). Notably, the *MT* locus in *dnmt1* strains showed substantial reduction in the repressive mark H3K9me1, while the levels of other modifications were unaltered (Fig. 5C), implying that the chromatin state has been compromised at *MT* in *dnmt1* strains. Collectively, *DNMT1* deficiency leads to the loss of 5mC, along with the reduction of H3K9me1 in a number of genetic loci including *MT*, potentially allowing access to recombination machinery.

Loss of H3K9me1 does not cause illegitimate recombination at *MT*

We wondered whether the decreased H3K9me1 level could directly contribute to the anomalous meiotic recombination phenotype in *dnmt1* mutants. SET3p (*Cre02.g089200*) is an H3K9 methyltransferase responsible for a high proportion (more than 60%) of H3K9 monomethylation in *C. reinhardtii* (17). By using the CRISPR-Cas9

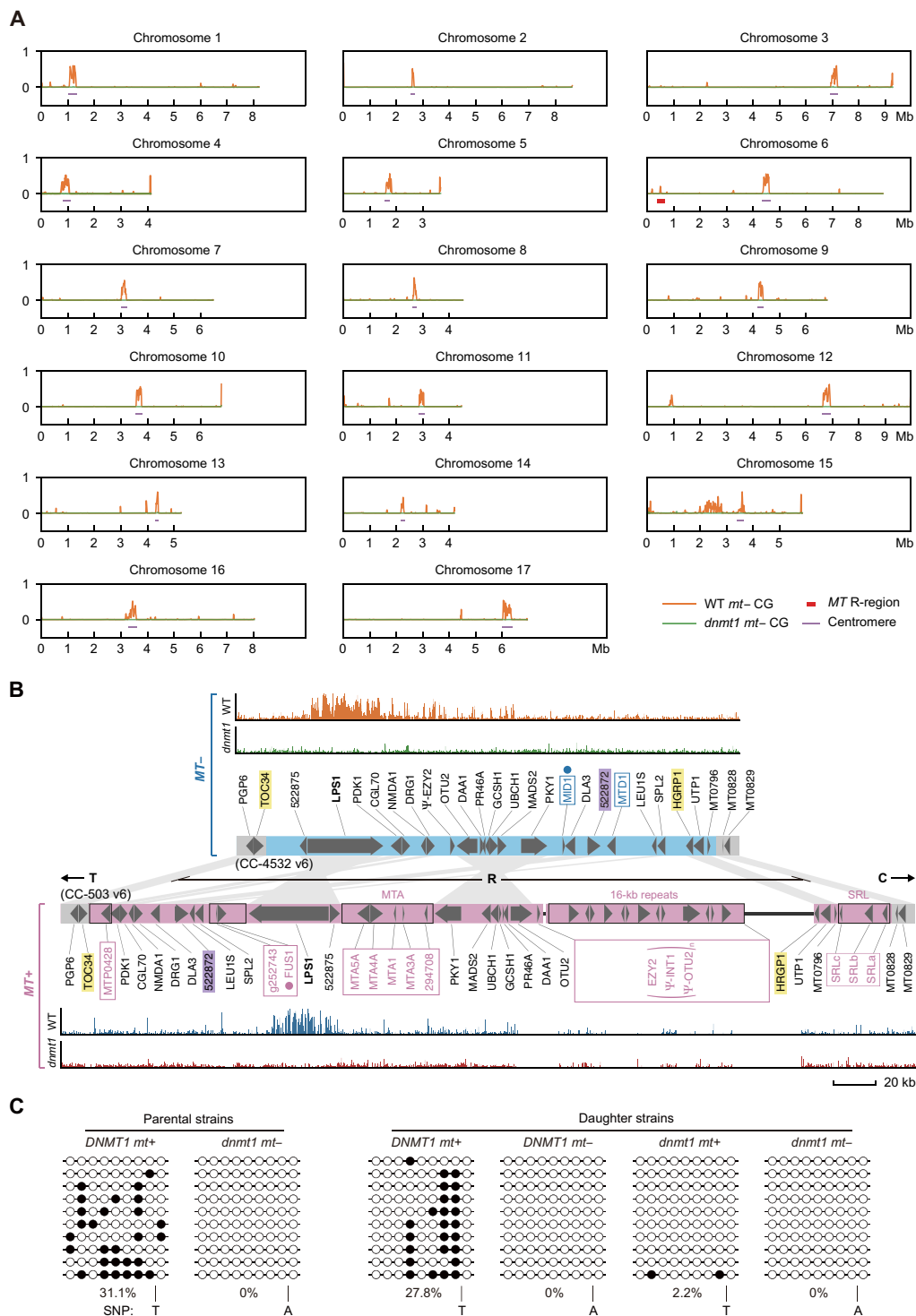


Fig. 4. Loss of 5mC at MT in the *dnmt1* strains. (A) 5mCG profiles across chromosomes in WT and *dnmt1* strains. The purple and red bars indicate centromeres previously reported (10) and MT in chromosome 6, respectively. WT (*mt*-) strain was CC-5325. *dnmt1* (*mt*-) strain was from *dnmt1* Ins2 strain (*mt*-) (Fig. 1C) backcrossed with WT CC-5155 (*mt*+). (B) Genome browser representation of 5mCGs at MT in WT and *dnmt1* strains of the two opposite mating types. The y axis in the tracks represents the ratio of 5mCGs to total CGs. T, telomere-proximal domain; R, rearranged domain; C, centromere-proximal domain. The diagram of the plus and minus alleles of the MT R-region was drawn on the basis of Craig *et al.* (10) Mating-type-specific gene symbols are boxed (blue for *mt*- and pink for *mt*+). (C) Methylation analysis by Sanger bisulfite sequencing of a selected R-region of MT (chromosome 6, 493,026 to 493,257 in CC-4532 V6 assembly) in WT (*mt*+), *dnmt1* Ins2 (*mt*-), and their four daughter strains. Blank and filled circles represent unmethylated CGs and 5mCGs, respectively. Letters T (from *mt*+) and A (from *mt*-) below represent a SNP present in the selected region, used to track the origin of the analyzed alleles between the parental strains.

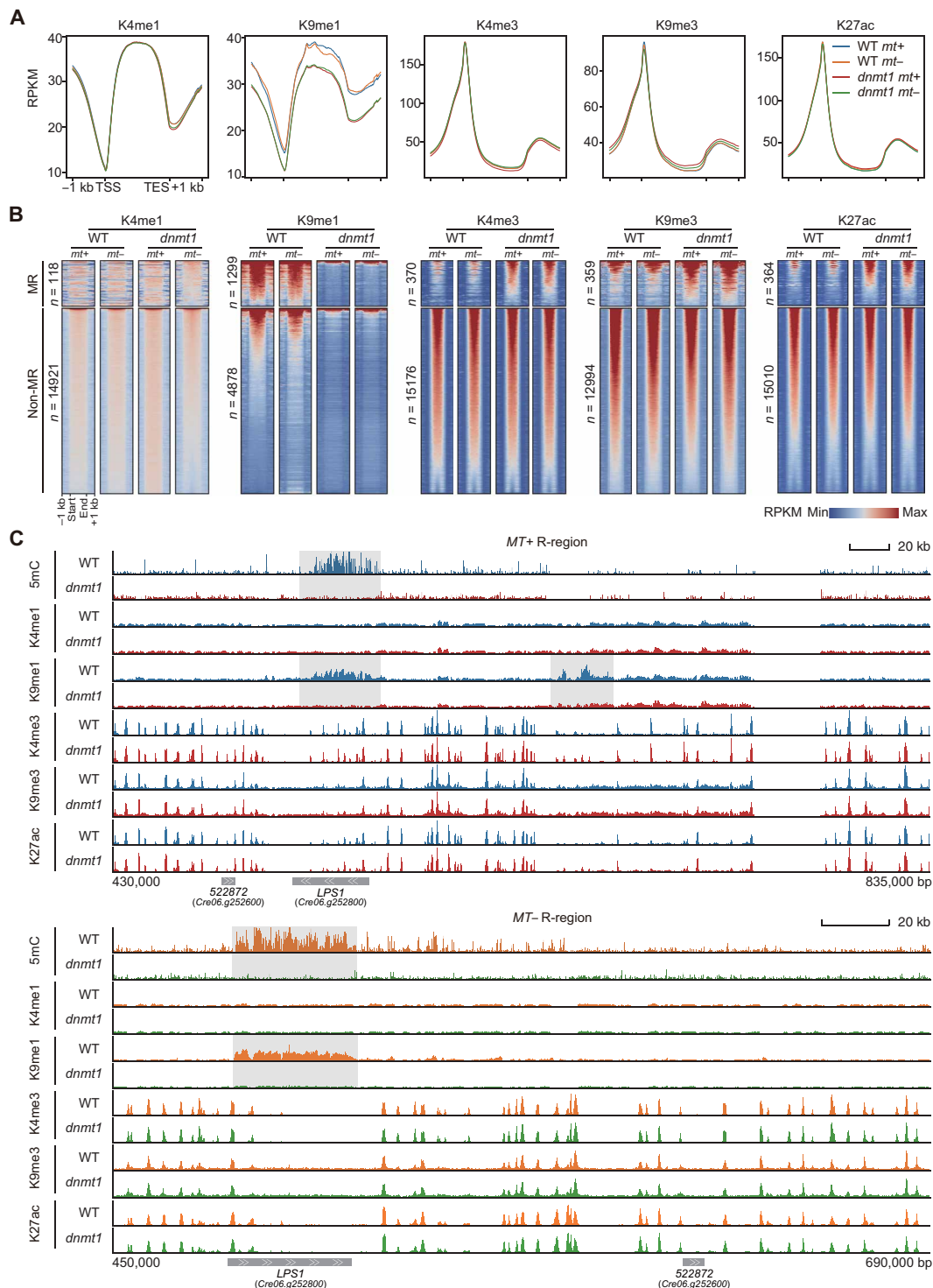


Fig. 5. Reduced H3K9me1 at MT in *dnmt1* strains. (A) Average H3K4me1, H3K9me1, H3K4me3, H3K9me3, and H3K27ac in ChIP-seq profiles of WT and *dnmt1* strains along the gene bodies of all annotated genes and 1-kb regions upstream and downstream of the gene body, respectively. TSS, transcription start site; TES, transcription end site; RPKM, reads per kilobase per million mapped reads. (B) Heatmap showing the H3K4me1, H3K9me1, H3K4me3, H3K9me3, and H3K27ac signals (in RPKM) around their peak regions. Peaks of each histone modification are divided into MRs and non-MR groups as illustrated. The number of genomic bins is displayed on the left. (C) Genome browser representation of 5mC, H3K4me1, H3K9me1, H3K4me3, H3K9me3, and H3K27ac in the MT R-region. For the track of 5mC, the y axis represents the ratio of 5mC to total C. For the tracks of histone marks, the y axis represents the normalized ChIP-seq reads in RPKM. The gray areas across the tracks highlight three sub-regions with the greatest variation in 5mC and H3K9me1 between WT and *dnmt1* strains. Two genes, *LPS1* harboring a high level of 5mC and 522872, in which recombination was identified are indicated.

gene editing method, we generated several insertional mutations in exon 3 of *SET3* (Fig. 6A). Through ChIP-seq, we found that, similar to the *dnmt1* strains, *set3* strains also showed global reduction of H3K9me1 at MRs including *MT* (Fig. 6, B and C). To examine the relationship between 5mC and H3K9me1 in *C. reinhardtii*, we quantified the 5mC level in *set3* strains by UHPLC-MS/MS and WGBS. Notably, the reduction of H3K9me1 in *set3* strains had little effect on the 5mC abundance (Fig. 6, C and D), suggesting that H3K9 monomethylation requires 5mC, but cytosine 5 methylation does not require H3K9me1.

We next asked whether the loss of H3K9me1 alone might be responsible for the meiosis defects in *dnmt1* strains. Spore viability and tetrad frequency of *set3* homozygotes were found similar to those of WT homozygotes (Fig. 6, E and F), suggesting that the recombination suppression of *MT* is independent of the level of H3K9me1.

These data indicate that the reduction of H3K9me1 at *MT* is a consequence of *dnmt1* deficiency but does not mediate the effect on meiotic recombination. On the basis of these data, we conclude that DNA methylation, rather than H3K9me1, is critical for recombination suppression at *MT* in *C. reinhardtii*.

DISCUSSION

Meiotic recombination in the SDRs is suppressed in various organisms through different mechanisms, including but not limited to sequence divergence/rearrangement and epigenetic modifications. For instance, histone H3K9 methylation is used for recombination suppression at the *MAT* locus in fission yeast, an organism that lacks DNA methylation (2). On the other hand, DNA methylation is enriched in the SDR in organisms such as sticklebacks and papaya (1),

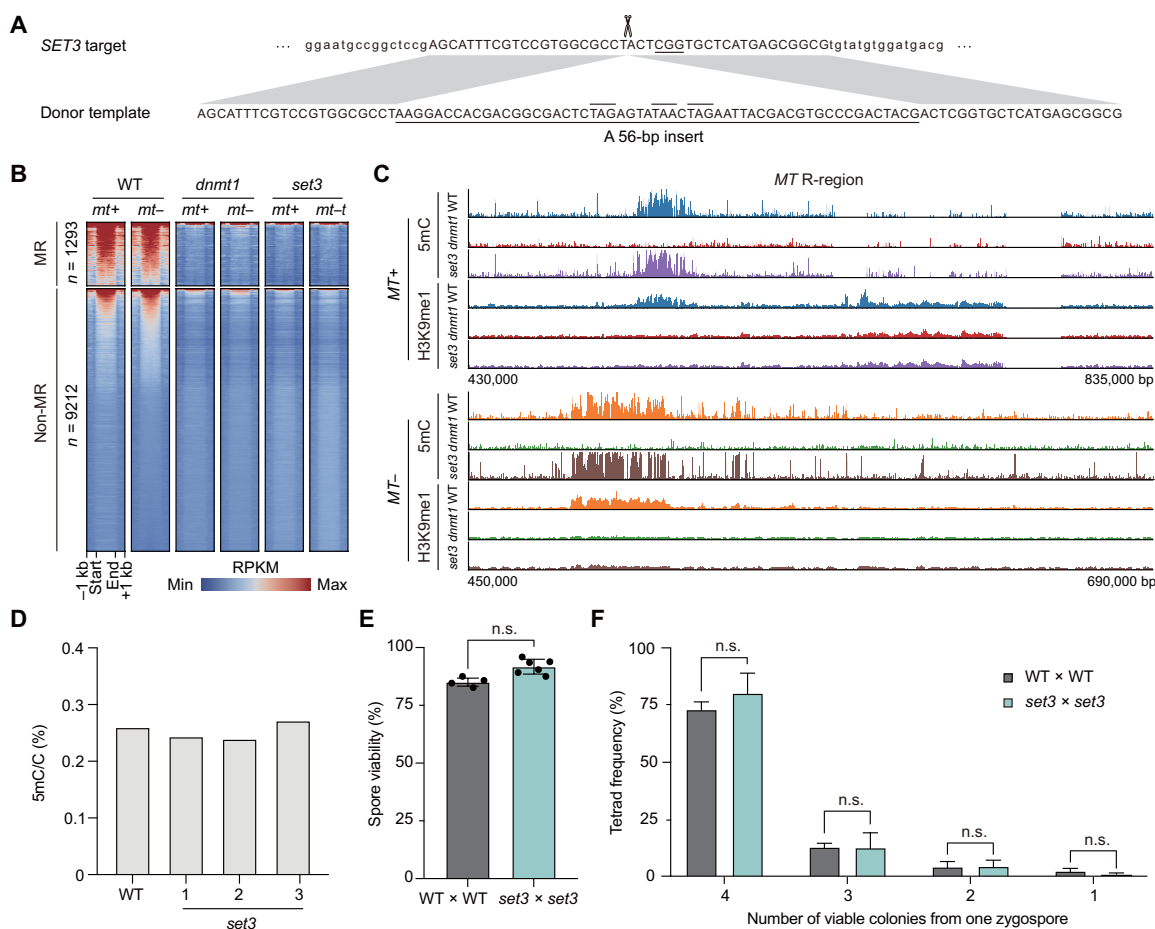


Fig. 6. Lack of meiotic defects in *set3* strains deficient in H3K9me1. (A) Generation of *set3* mutant strains by targeted gene inactivation using CRISPR-Cas9 technology in WT CC-5325 strain. A 56-bp insert containing three stop codons (overlined) is introduced into exon 3 of the *SET3* gene by microhomologous recombination of the indicated donor template. The PAM is underlined. The Cas9 cleavage site is indicated with scissors. (B) Heatmap showing the H3K9me1 signals (in RPKM) around its peak regions. Peaks are divided into two groups: MRs and non-MRs. (C) Genome browser representation of 5mC level and H3K9me1 profile of six indicated strains in the *MT* R-region. For the track of 5mC, the y axis represents the ratio of 5mC to total C. For the tracks of H3K9me1, the y axis represents the normalized ChIP-seq reads in RPKM. (D) 5mC contents in the genomic DNA from WT CC-5325 strain and three independent *set3* mutant strains quantified by MS. (E) Spore viability of WT and *set3* homozygotes. Spore viability is calculated by dividing the number of viable spore colonies by the number of total spores placed on the plate. WT (*mt+*) and WT (*mt-*) are CC-5155 strain and CC-5325 strain; *set3* (*mt+*) and *set3* (*mt-*) are the progenies of *set3* strains (D) backcrossed with WT CC-5155 strain. (F) Frequency of tetrads with one to four viable spore(s) in two cross sets indicated. ((E) and (F)) Data are means \pm SEM from four or six independent biological replicates. Two-tailed Student's *t* test was used without adjustment for multiple comparisons.

raising the possibility that DNA methylation controls recombination suppression in these organisms. In this study, we provide evidence that meiotic recombination at *MT* locus is suppressed by DNA cytosine methylation but not H3K9 methylation in *C. reinhardtii*, thus revealing a novel mechanism for recombination suppression of the SDR in eukaryotes. In WT *C. reinhardtii* meiotic cells, recombination at the rearranged sequence of *MT* is suppressed efficiently, though there is evidence of occasional gene conversion (18). Notably, when strains were constructed that could mate with a partner that had the same *MT* haplotype (*mt+::MID1*, *mt- mid1*), recombination within *MT* was restored in *mt+ × mt+* crosses but was still suppressed in *mt- × mt-* crosses (18) implying that rearrangements alone were not responsible for suppressing recombination within *MT* and that suppression might be mediated through sequences or epigenetic modifications in *mt-*. Our data are consistent with this finding and further suggest that DNA methylation is the mediator of active recombination suppression within the *MT* locus of *C. reinhardtii*.

Although we have demonstrated that cytosine methylation is instrumental in suppressing the meiotic recombination at *MT*, it is unclear how deficiency in 5mC leads to the aberrant *MT* recombination. There are at least three plausible mechanisms. First, 5mC deficiency makes the local chromatin regions more accessible to recombination factors. Prevention of chromatin accessibility perhaps depends on 5mC itself and/or protein(s) recruited by 5mC. Although the chromatin at *MT* is speculated to become more accessible in *dnmt1* strains, the local chromatin state is far from characterized. Future efforts will be needed to develop sensitive genomic and epigenomic procedures amenable to zygospores. A hurdle to overcome is to isolate sufficient zygospores undergoing meiosis, which has also precluded analyses of the methylome and transcriptome. Second, derivatives of 5mC, rather than 5mC, might be implicated in mediating recombination suppression at *MT*. We previously uncovered a new cytosine modification, 5-glyceryl-methylcytosine (5gmC), which counteracts DNA methylation in the regulation of photosynthesis in *C. reinhardtii* (19). *dnmt1* strains have a diminished level of 5mC and are expected to also have reduced 5gmC or other unknown 5mC derivatives. Third, 5mC loss may lead to misregulation of genes associated with recombination suppression at *MT*. In this vein, it is worth emphasizing that none of the genes presumably involved in meiotic recombination exhibited notable dysregulation in *dnmt1* strains in the vegetative stage (fig. S7, A to C). Furthermore, the alterations in the expression of *MT* locus genes were minimal, even in the presence of comprehensive 5mC loss (fig. S7D). This finding highlights that DNA methylation may not be a primary mediator of gene silencing in *C. reinhardtii* as it is in other species but may have a more restricted role in suppressing recombination at *MT* and perhaps other loci. The identification of DNA binding proteins for 5mC and its derivatives may be the key to uncovering the precise underlying cause of the aberrant *MT* meiotic recombination in *dnmt1* strains.

The location within *MT* prone to anomalous recombination does not appear random. In all seven mixed-*mt* strains obtained, recombination is localized within the unmethylated gene 522872 (fig. S3). It is also important to note that the illegitimate recombination that occurred in *dnmt1* was through a homology-dependent mechanism and that the 522872 gene is in the same orientation on chromosome 6 in both mating types but in different relative positions within the R-region of each mating haplotype. This allowed one chromatid in

the reciprocal exchange to maintain at least one copy of all *MT* genes and survive, while the other lost several genes and presumably caused spore inviability after meiotic segregation (refer to Fig. 4B). It is possible that homology-driven crossovers also occur in inverted regions within the two *MT* haplotypes, but these would be expected to generate inviable products in both chromatids undergoing exchange and would not be recovered. Last, the 522782 gene may also be a recombination hotspot within *MT*, and DNA methylation of the adjacent *LPS1* gene counteracts this effect.

As the most prevalent epigenetic marks of transcriptionally silenced heterochromatin, histone H3K9 methylation is conserved among diverse organisms (20). Our data suggest that while DNA methylation influences H3K9 methylation, altered H3K9 methylation is insufficient to explain recombination suppression at *MT*. This is evidenced by the fact that a mutation in the *SET3* methyltransferase gene that blocked H3K9 methylation without affecting DNA methylation had no impact on *MT* recombination. Nevertheless, the overall contribution of a local chromatin state to the control of the *MT* recombination remains poorly understood. While many types of histone modifications are conserved, their epigenetic consequences appear different in *C. reinhardtii*. For instance, H3K4me1 primes enhancers in mammals (21) but serves as a repressive mark in *C. reinhardtii* (17, 22, 23), while H3K9me3 is a repressive mark in mammals but functions as an active mark in the alga (17). Enzymes for most algal histone modifications have not been characterized. Meanwhile, there is a puzzling enigma in *C. reinhardtii* that maintains a high global abundance of putatively repressive histone marks but most of the genes remain in an active state at most cell cycle stages (15). Further studies are warranted to elucidate how DNA and histone modifications are orchestrated to regulate the *MT* in *C. reinhardtii*.

From an evolutionary point of view, the emergence of DNA modification might have preceded histone-based chromatin modifications, given that DNA modifications are ubiquitous in viruses and archaeans independent of packaging their genomes in chromatin (3). On the basis of our findings in *C. reinhardtii*, we surmise that the ancestral single-celled eukaryotes having evolved ~2 billion years ago, in the absence of present-day elaborate nucleosome assembly, might have taken advantage of DNA modifications for recombination suppression of SDRs so that adaptation and evolution through sexual reproduction would be possible. It would be interesting to examine whether DNA methylation is required for recombination suppression of SDR in diverse lineages such as mammals in which the XY pair is largely nonpermissive for recombination in spermatocytes (24, 25).

MATERIALS AND METHODS

C. reinhardtii strains and gene editing

The insertion mutants *Cre10.g461750* (LMJ.RY0402.088494), *Cre03.g200750* (LMJ.RY0402.153527), and *Cre03.g202150* (LMJ.RY0402.085731) were obtained from the *Chlamydomonas* mutant library (CLiP, www.chlamylibrary.org/). Their corresponding WT strain CC-5155/CC-5325 and the polymorphic strain CC-1952 (*mt-*, alias S1-C5) were provided by the *Chlamydomonas* Resource Center (<http://chlamycollection.org/strains/>). The *dnmt1* Exon2 insertion, *dnmt1* C1830S point mutation, and *set3* Exon3 insertion strains were generated by gene editing using a CRISPR-Cas9 system in CC-5325 background (26). The *dnmt1* (*mt+*) and *dnmt1* (*mt-*) strains for phenotype characterization were derived from *dnmt1* Ins1 strain (Fig. 1C) and *dnmt1* Ins2 strain (Fig. 1C), backcrossed with WT CC-5155 strain,

five times and once, respectively. The *set3* (*mt+*) and *set3* (*mt-*) strains for phenotype characterization were the progenies of *set3* strains (Fig. 6D) backcrossed with WT CC-5155 strain.

Cell culture conditions

Cells were grown photomixotrophically in liquid tris-acetate-phosphate (TAP) medium on a rotary shaker at 22° to 25°C or on agar-solidified TAP medium under continuous light (50 to 100 $\mu\text{E m}^{-2} \text{s}^{-1}$, cool-white fluorescent lamps). Cell numbers were determined by counting of 100-fold diluted samples in a Z2 Coulter Counter (Beckman Coulter, Krefeld, Germany).

Extraction of genomic DNA

To isolate genomic DNA, the procedure was adopted from the Plant Genomic DNA Kit (catalog no. DP305-03, Tiangen) as follows: Vegetative cells were grown in 100 ml of TAP medium to stationary phase and harvested by centrifugation (5 min, 4200 rpm, room temperature). The cell pellet was resuspended in Buffer GD from the kit. The suspension was transferred into lysing matrix E (catalog no. 116914050, MP Biomedicals) and then incubated for 15 min at 65°C, 1400 rpm. The ensuing steps followed the kit's protocol.

UHPLC-MS/MS analysis

In brief, purified high-quality DNA was digested by nuclease P1 (catalog no. N8630, Sigma-Aldrich) in the presence of 0.2 mM ZnSO_4 and 20 mM NaAc (pH 5.3) at 55°C for at least 4 hours and then was dephosphorylated with calf intestinal alkaline phosphatase (catalog no. 2250A, Takara) at 37°C for at least 4 hours. The samples were centrifuged at maximum speed in a microcentrifuge for 5 min, and the supernatants were then subjected to UHPLC-MS/MS analysis for quantitation of 5mC. The UHPLC-MS/MS analyses were performed using a UHPLC system (Agilent Technologies, 1290 series) coupled to a triple quadrupole mass spectrometer (AB, SCIEX QTRAP 6500+).

Bisulfite sequencing

For bisulfite sequencing, genomic DNA was treated with the EZ DNA Methylation-Direct Kit (catalog no. D5021, Zymo). The bisulfite-treated DNA was subjected to PCR amplification using Taq HS polymerase (catalog no. R007B, Takara). PCR products were then purified with a Gel Extraction Kit (catalog no. 28706, Qiagen) and cloned into a pClone007 Simple Vector (catalog no. TSV-007S, Tsingke). Individual clones were sequenced by standard Sanger sequencing. Data were analyzed using the online tool QUMA (<http://quma.cdb.riken.jp/>).

WGBS data analysis

Whole-genome bisulfite DNA sequencing was performed on *C. reinhardtii* WT (*mt+*), WT (*mt-*), *dnmt1* (*mt+*), and *dnmt1* (*mt-*) strains. As a control for bisulfite conversion, unmethylated lambda DNA was used as spike-in to calculate the conversion failure rate. Bisulfite-converted sequences were aligned to *C. reinhardtii* (CC-4532 v6) nuclear genome, chloroplast genome, mitochondria genome, and lambda DNA using the Bismark alignment pipeline (version: v0.22.3) (27). Methylation (0.21%) was typically detected in unmethylated lambda, indicating a conversion efficiency of 99.79%. GlobalMethLev in ViewBS R package (28) was used to generate weighted DNA methylation levels for the samples. To map the distribution and enrichment of 5mC in the genome, MethGeno in ViewBS R package was used to

generate the methylation levels across each chromosome. Then, a sliding window of 20 kb in size was used to generate the DNA methylation profiles for genome browser visualization, with a step size of 10 kb along chromosomes. Differentially methylated regions (DMRs) were identified by DSS (29) with parameter *P* value = 0.05, minimum change in the fraction of methylated CpG sites ($\Delta 5\text{mCG}$) = 0.1, minimum length (in base pairs) required for $\text{DMR} = 20$, minimum number of CpG sites required for $\text{DMR} = 2$. Neighboring DMRs were merged into one if they were within 2000 base pairs of one another and had methylation changes in the same direction. Furthermore, the merged DMRs displaying an average change in 5mCG level ($|\Delta 5\text{mCG}| < 0.05$) which showed poor consistency between replicates were not used for the following analyses. The finalized DMRs are presented in table S2. Notably, given the near-absent methylation rates observed in the *dnmt1* strains (as shown in Figs. 1C and 4A, fig. S6B, and table S2), these DMRs were characterized as MRs in the WT strains. The gff3 file containing annotations of repetitive sequences, as identified by RepeatMasker, was sourced from Phytozome (Annotation-version CC-4532 v6.1). CC-4532 v6 served as the primary reference genome throughout this study. When visualizing the methylation track of the *MT+* locus, CC-503 v6 (*mt+*) assembly was used as the reference genome.

Mating and tetrad analysis

Gametogenesis, mating, and tetrad analysis were performed by standard procedures described previously (30). The dissected progenies were grown under appropriate conditions until visible colonies could be picked for subsequent analysis. All data are shown in table S3.

Mating ability test

Mating ability test was performed by standard procedures described previously (31, 32).

Quantification of chromatin copy number by quantitative real-time PCR

Vegetative cells were grown to a cell density of $2 \times 10^6 \text{ ml}^{-1}$ in TAP medium, and 2×10^6 cells were harvested by centrifugation (3 min, 12,000 rpm, 4°C). The cell pellet was lysed in 50 μl of PD1 buffer (catalog no. AD301, Transgen) at 95°C for 20 min, and the lysing stopped by the addition of 50 μl of PD2 buffer (catalog no. AD301, Transgen). After 15-min centrifugation at 13,300 rpm and 4°C, the supernatant was collected as real-time PCR template, which was diluted 128-fold to ensure the cycle threshold was within an appropriate range.

SNP calling

Whole-genome sequencing was conducted on strains #1-1 (*mt+*), #1-2 (*mt-*), #1-3 (*mt+/-*), *dnmt1* (*mt+*), *dnmt1* (*mt-*), #2-3 (*mt+/-*), #3-1 (*mt+/-*), #4-1 (*mt+/-*), #5-1 (*mt+/-*), #6-1 (*mt+/-*), and #7-2 (*mt+/-*). The reads were aligned to the reference sequence of *C. reinhardtii* (CC-4532 v6) using BWA (version 0.7) (33). The resulting SAM files were converted to a BAM format and sorted using SAMtools (version 1.7) (34). Duplicated reads were eliminated using Picard MarkDuplicates (<https://broadinstitute.github.io/picard/>). Subsequently, the Samtools mpileup generated pileup format files, which were then subjected to VarScan's mpileup2snp command (35) for detecting SNPs. In the initial step, we excluded SNPs with mutation rates below 90% in strains #1-1 (*mt+*) and #1-2 (*mt-*) or *dnmt1* (*mt+*) and *dnmt1* (*mt-*), followed by the identification of specific

SNPs that discriminate between the *mt+* and *mt-* parental strains on the basis of nucleotide disparities observed between #1-1 and #1-2 or *dnmt1* (*mt+*) and *dnmt1* (*mt-*). Subsequently, SNPs in all *mt+/-* strains exhibiting the rates below 40% were excluded as potential false positives. The remaining SNPs were then used to delineate parental inheritance patterns.

Chromatin immunoprecipitation sequencing

ChIP was performed as previously described (36) with changes as follows. Antibodies specific for the following epitopes were used for each sample: H3K4me1 (5 μ l, ab8895), H3K9me1 (5 μ l, ab9045), H3K4me3 (5 μ l, ab8580), H3K9me3 (5 μ l, CST 13969 T), and H3K27ac (5 μ l, ab4729). Antibody-protein/DNA complexes were allowed to form during a 4-hour incubation at 4°C, complexed with 40 μ l of Dynabeads Protein G (30 mg/ml, Invitrogen) after washing twice with dilution buffer during a 2-hour incubation at 4°C. ChIPed DNA (1 ng) was used for library preparation (catalog no. ND607, Vazyme). Libraries were pooled and sequenced on the Illumina NovaSeq 6000 system at 2 \times 150 bp.

ChIP-seq data processing

Raw reads were trimmed from the 3' end to have a phred score of at least 20. Illumina sequencing adapters were removed from the reads using Trim galore (version 0.6.7, www.bioinformatics.babraham.ac.uk/projects/trim_galore/). Each read was mapped against the *C. reinhardtii* reference sequence (CC-4532 v6) using Bowtie 2 version 2.4.2 (37). SAMtools was then used to convert SAM files to sorted and indexed BAM files. Duplicate reads were removed by Picard MarkDuplicates. Coverage tracks and heatmap of ChIP-seq signal were generated from aligned reads using deepTools (version 3.5.1) (38). The coverage was calculated as the number of reads per 200 bp bin and normalized to reads per kilobase per million mapped reads, and the reads mapped to nonpeak regions in individual samples were used to calculate scale factors. The CC-503 v6 (*mt+*) assembly was used as the reference genome solely for the purpose of representing the track of histone marks within the *MT+* locus.

ChIP-seq peak calling

Peaks were called for each pooled or individual samples using MACS2 version 2.2.7.1 (39) using the following parameters “-g 114000000, -q 0.01.” MANorm2_utils was used for processing a set of ChIP-seq samples into a regular table recording a list of union genomic bins, and the parameter typical bin size was set to 5000 for broad (H3K4me1 and H3K9me1) and 2000 for narrow (H3K4me3, H3K9me3, and H3K27ac) histone modifications (40).

Extraction of total RNA

To obtain total RNA for RNA sequencing (RNA-seq), the procedure was adopted from the KK Fast Plant Total RNA Kit (catalog no. ZP405K, Zomanbio) as follows: Vegetative cells were grown to a cell density of 2 \times 10⁶ ml⁻¹ in TAP medium, and 1 \times 10⁷ cells were harvested by centrifugation (3 min, 2500 rpm, 4°C). The cell pellet was resuspended in 1 ml of TRIzol (Thermo Fisher Scientific). The ensuing steps in the procedure followed the kit's protocol.

RNA-seq data analysis with DESeq2

After removal of adaptor contamination, sequencing reads were aligned using STAR (version 2.7.6) (41) to *C. reinhardtii* reference sequence (CC-4532 Assembly-version = v6, Annotation-version = v6.1) and

feature Counts were used to produce a matrix of counts by genes. After removing features with zero counts across all samples, the raw counts were normalized with DESeq2 (42). Differentially expressed genes were identified using DESeq2 with a *P* value <0.05 and estimated fold change >2.

Supplementary Materials

The PDF file includes:

Figs. S1 to S7

Legends for tables S1 to S3

Other Supplementary Material for this manuscript includes the following:

Tables S1 to S3

REFERENCES AND NOTES

- B. L. S. Furman, D. C. H. Metzger, I. Darolti, A. E. Wright, B. A. Sandkam, P. Almeida, J. J. Shu, J. E. Mank, Sex chromosome evolution: So many exceptions to the rules. *Genome Biol. Evol.* **12**, 750–763 (2020).
- J. Oh, S. Yeom, J. Park, J. S. Lee, The regional sequestration of heterochromatin structural proteins is critical to form and maintain silent chromatin. *Epigenetics Chromatin* **15**, 5 (2022).
- C. F. Brunk, W. F. Martin, Archaeal histone contributions to the origin of eukaryotes. *Trends Microbiol.* **27**, 703–714 (2019).
- U. Goodenough, H. Lin, J. H. Lee, Sex determination in *Chlamydomonas*. *Semin. Cell Dev. Biol.* **18**, 350–361 (2007).
- P. J. Ferris, U. W. Goodenough, The mating-type locus of *Chlamydomonas reinhardtii* contains highly rearranged DNA sequences. *Cell* **76**, 1135–1145 (1994).
- D. Schubeler, Function and information content of DNA methylation. *Nature* **517**, 321–326 (2015).
- K. Skvortsova, O. Bogdanovic, TAB-seq and ACE-seq data processing for genome-wide DNA hydroxymethylation profiling. *Methods Mol. Biol.* **2272**, 163–178 (2021).
- D. Lopez, T. Hamaji, J. Kropat, P. De Hoff, M. Morselli, L. Rubbi, S. Fitz-Gibbon, S. D. Gallaher, S. S. Merchant, J. Umen, M. Pellegrini, Dynamic changes in the transcriptome and methylome of *Chlamydomonas reinhardtii* throughout its life cycle. *Plant Physiol.* **169**, 2730–2743 (2015).
- X. Li, W. Patena, F. Fauser, R. E. Jinkerson, S. Saroussi, M. T. Meyer, N. Ivanova, J. M. Robertson, R. Yue, R. Zhang, J. Vilarrasa-Blasi, T. M. Wittkopp, S. Ramundo, S. R. Blum, A. Goh, M. Laudon, T. Srikumar, P. A. Lefebvre, A. R. Grossman, M. C. Jonikas, A genome-wide algal mutant library and functional screen identifies genes required for eukaryotic photosynthesis. *Nat. Genet.* **51**, 627–635 (2019).
- R. J. Craig, S. D. Gallaher, S. Shu, P. A. Salome, J. W. Jenkins, C. E. Blaby-Haas, S. O. Purvine, S. O'Donnell, K. Barry, J. Grimwood, D. Strenkert, J. Kropat, C. Daum, Y. Yoshinaga, D. M. Goodstein, O. Vallon, J. Schmutz, S. S. Merchant, The *Chlamydomonas* Genome Project, version 6: Reference assemblies for mating-type *plus* and *minus* strains reveal extensive structural mutation in the laboratory. *Plant Cell* **35**, 644–672 (2023).
- G. Farkas, B. A. Leibovitch, S. C. Elgin, Chromatin organization and transcriptional control of gene expression in *Drosophila*. *Gene* **253**, 117–136 (2000).
- M. V. C. Greenberg, D. Bourchis, The diverse roles of DNA methylation in mammalian development and disease. *Nat. Rev. Mol. Cell Biol.* **20**, 590–607 (2019).
- J. H. Waterborg, A. J. Robertson, D. L. Tatar, C. M. Borza, J. R. Davie, Histones of *Chlamydomonas reinhardtii*. Synthesis, acetylation, and methylation. *Plant Physiol.* **109**, 393–407 (1995).
- K. van Dijk, K. E. Marley, B. R. Jeong, J. Xu, J. Hesson, R. L. Cerny, J. H. Waterborg, H. Cerutti, Monomethyl histone H3 lysine 4 as an epigenetic mark for silenced euchromatin in *Chlamydomonas*. *Plant Cell* **17**, 2439–2453 (2005).
- S. R. Rommelfanger, M. Zhou, H. Shaghias, S. C. Tzeng, B. S. Evans, L. Pasa-Tolic, J. G. Umen, J. J. Pesavento, An improved top-down mass spectrometry characterization of *Chlamydomonas reinhardtii* histones and their post-translational modifications. *J. Am. Soc. Mass Spectrom.* **32**, 1671–1688 (2021).
- D. Strenkert, A. Yildirim, J. Yan, Y. Yoshinaga, M. Pellegrini, R. C. O'Malley, S. S. Merchant, J. G. Umen, The landscape of *Chlamydomonas* histone H3 lysine 4 methylation reveals both constant features and dynamic changes during the diurnal cycle. *Plant J.* **112**, 352–368 (2022).
- J. A. Casas-Mollano, K. van Dijk, J. Eisenhart, H. Cerutti, SET3p monomethylates histone H3 on lysine 9 and is required for the silencing of tandemly repeated transgenes in *Chlamydomonas*. *Nucleic Acids Res.* **35**, 939–950 (2007).
- P. L. De Hoff, P. Ferris, B. J. Olson, A. Miyagi, S. Geng, J. G. Umen, Species and population level molecular profiling reveals cryptic recombination and emergent asymmetry in the dimorphic mating locus of *C. reinhardtii*. *PLOS Genet.* **9**, e1003724 (2013).

19. J. H. Xue, G. D. Chen, F. Hao, H. Chen, Z. Fang, F. F. Chen, B. Pang, Q. L. Yang, X. Wei, Q. Q. Fan, C. Xin, J. Zhao, X. Deng, B. A. Wang, X. J. Zhang, Y. Chu, H. Tang, H. Yin, W. Ma, L. Chen, J. Ding, E. Weinhold, R. M. Kohli, W. Liu, Z. J. Zhu, K. Huang, H. Tang, G. L. Xu, A vitamin-C-derived DNA modification catalysed by an algal TET homologue. *Nature* **569**, 581–585 (2019).
20. J. Nakayama, J. C. Rice, B. D. Strahl, C. D. Allis, S. I. Grewal, Role of histone H3 lysine 9 methylation in epigenetic control of heterochromatin assembly. *Science* **292**, 110–113 (2001).
21. H. Kang, M. N. Shokhirev, Z. Xu, S. Chandran, J. R. Dixon, M. W. Hetzer, Dynamic regulation of histone modifications and long-range chromosomal interactions during postmitotic transcriptional reactivation. *Genes Dev.* **34**, 913–930 (2020).
22. C. Y. Ngan, C. H. Wong, C. Choi, Y. Yoshinaga, K. Louie, J. Jia, C. Chen, B. Bowen, H. Cheng, L. Leonelli, R. Kuo, R. Baran, J. G. Garcia-Cerdan, A. Pratap, M. Wang, J. Lim, H. Tice, C. Daum, J. Xu, T. Northen, A. Visel, J. Bristow, K. K. Niyogi, C. L. Wei, Lineage-specific chromatin signatures reveal a regulator of lipid metabolism in microalgae. *Nat. Plants* **1**, 15107 (2015).
23. M. Schroda, Good news for nuclear transgene expression in *Chlamydomonas*. *Cells* **8**, 1534 (2019).
24. M. A. Handel, The XY body: An attractive chromatin domain. *Biol. Reprod.* **102**, 985–987 (2020).
25. J. M. Turner, Meiotic silencing in mammals. *Annu. Rev. Genet.* **49**, 395–412 (2015).
26. H. Chen, Q. L. Yang, J. X. Xu, X. Deng, Y. J. Zhang, T. Liu, M. G. Rots, G. L. Xu, K. Y. Huang, Efficient methods for multiple types of precise gene-editing in *Chlamydomonas*. *Plant J.* **115**, 846–865 (2023).
27. F. Krueger, S. R. Andrews, Bismark: A flexible aligner and methylation caller for Bisulfite-Seq applications. *Bioinformatics* **27**, 1571–1572 (2011).
28. X. Huang, S. Zhang, K. Li, J. Thimmapuram, S. Xie, J. Wren, ViewBS: A powerful toolkit for visualization of high-throughput bisulfite sequencing data. *Bioinformatics* **34**, 708–709 (2018).
29. H. Feng, H. Wu, Differential methylation analysis for bisulfite sequencing using DSS. *Quant. Biol.* **7**, 327–334 (2019).
30. X. Jiang, D. Stern, Mating and tetrad separation of *Chlamydomonas reinhardtii* for genetic analysis. *J. Vis. Exp.* 10.3791/1274, (2009).
31. C. F. Beck, A. Acker, Gametic Differentiation of *Chlamydomonas reinhardtii*: Control by nitrogen and light. *Plant Physiol.* **98**, 822–826 (1992).
32. N. Muller, S. Wenzel, Y. Zou, S. Kunzel, S. Sasso, D. Weiss, K. Prager, A. Grossman, T. Kottke, M. Mittag, A plant cryptochrome controls key features of the *Chlamydomonas* circadian clock and its life cycle. *Plant Physiol.* **174**, 185–201 (2017).
33. H. Li, R. Durbin, Fast and accurate short read alignment with Burrows-Wheeler transform. *Bioinformatics* **25**, 1754–1760 (2009).
34. P. Danecek, J. K. Bonfield, J. Liddle, J. Marshall, V. Ohan, M. O. Pollard, A. Whitwham, T. Keane, S. A. McCarthy, R. M. Davies, H. Li, Twelve years of SAMtools and BCFtools. *Gigascience* **10**, giab008 (2021).
35. D. C. Koboldt, Q. Zhang, D. E. Larson, D. Shen, M. D. McLellan, L. Lin, C. A. Miller, E. R. Mardis, L. Ding, R. K. Wilson, VarScan 2: Somatic mutation and copy number alteration discovery in cancer by exome sequencing. *Genome Res.* **22**, 568–576 (2012).
36. D. Strenkert, S. Schmollinger, M. Schroda, Protocol: Methodology for chromatin immunoprecipitation (ChIP) in *Chlamydomonas reinhardtii*. *Plant Methods* **7**, 35 (2011).
37. B. Langmead, C. Trapnell, M. Pop, S. L. Salzberg, Ultrafast and memory-efficient alignment of short DNA sequences to the human genome. *Genome Biol.* **10**, R25 (2009).
38. F. Ramirez, F. Dunder, S. Diehl, B. A. Gruning, T. Manke, deepTools: A flexible platform for exploring deep-sequencing data. *Nucleic Acids Res.* **42**, W187–W191 (2014).
39. Y. Zhang, T. Liu, C. A. Meyer, J. Eeckhoutte, D. S. Johnson, B. E. Bernstein, C. Nusbaum, R. M. Myers, M. Brown, W. Li, X. S. Liu, Model-based analysis of ChIP-Seq (MACS). *Genome Biol.* **9**, R137 (2008).
40. S. Tu, M. Li, H. Chen, F. Tan, J. Xu, D. J. Waxman, Y. Zhang, Z. Shao, MAnorm2 for quantitatively comparing groups of ChIP-seq samples. *Genome Res.* **31**, 131–145 (2021).
41. A. Dobin, C. A. Davis, F. Schlesinger, J. Drenkow, C. Zaleski, S. Jha, P. Batut, M. Chaisson, T. R. Gingeras, STAR: Ultrafast universal RNA-seq aligner. *Bioinformatics* **29**, 15–21 (2013).
42. M. I. Love, W. Huber, S. Anders, Moderated estimation of fold change and dispersion for RNA-seq data with DESeq2. *Genome Biol.* **15**, 550 (2014).
43. I. Zamora, J. L. Feldman, W. F. Marshall, PCR-based assay for mating type and ploidy in *Chlamydomonas*. *Biotechniques* **37**, 534–536 (2004).

Acknowledgments: We thank R. J. Craig, L. Du, X. He, J. Mank, F. Li, and J. Song for critical reading and discussion of the manuscript. **Funding:** This work was supported by grants from the National Natural Science Foundation of China (31991163, 82088101, and 31830018 to G.-L.X.), Shanghai Municipal Science and Technology Major Project (to G.-L.X.), the Sino-German Mobility Program (M-0313 to G.-L.X.), and the National Natural Science Foundation of China (32370576 to H.C.). H.C. gratefully acknowledges the support of the SANOFI Scholarship Program. **Author contributions:** Conceptualization: G.-L.X. Methodology: T.G., W.X., X.G., Z.S., and G.-L.X. Investigation: T.G., W.X., J.-X.X., and C.-H.W. Visualization: G.-L.X. and G.-L.X. Funding acquisition: G.-L.X. and H.C. Project administration: G.-L.X. and Z.S. Supervision: G.-L.X., Y.-R.D., and H.C. Writing—original draft: T.G., X.G., W.X., Y.-R.D., H.C., Z.S., and G.-L.X. Writing—review and editing: J.G.U., K.H., W.Y. C.W., and J.W. **Competing interests:** The authors declare that they have no competing interests. **Data and materials availability:** All data needed to evaluate the conclusions in the paper are present in the paper and/or the Supplementary Materials. The raw and processed ChIP-seq, RNA-seq, and WGBS data files generated during this study are available at the NCBI under GEO accession number GSE245614. The whole-genome sequencing data of the daughter strains generated in this study are deposited under NCBI BioProject PRJNA1110635. Software and code used in this study are referenced in their corresponding STAR Method sections.

Submitted 21 June 2024
 Accepted 4 September 2024
 Published 9 October 2024
 10.1126/sciadv.adr2345